Global Biogeochemical Cycles®

AGU ADVANCING EARTH AND SPACE SCIENCE

RESEARCH ARTICLE
10.1029/2022GB007371

Key Points:

- Export fluxes of 15 trace elements reveal contrasted seasonal patterns between lithogenic and biological carriers
- Basalt particles are the major lithogenic carrier phase of trace elements
- Fecal pellets, diatom vegetative cells and spores are each carriers of distinct trace elements

Supporting Information:

Supporting Information may be found in the online version of this article.

Correspondence to:

S. Blain,
stephane.blain@obs-banyuls.fr

Citation:

Blain, S., Planquette, H., Obernosterer, I., & Guéneuguès, A. (2022). Vertical flux of trace elements associated with lithogenic and biogenic carrier phases in the Southern Ocean. *Global Biogeochemical Cycles*, *36*, e2022GB007371. https://doi.org/10.1029/2022GB007371

Received 3 MAR 2022
Accepted 28 APR 2022

Author Contributions:

Conceptualization: S. Blain
Data curation: S. Blain, A. Guéneuguès
Formal analysis: S. Blain, H. Planquette, I. Obernosterer
Funding acquisition: S. Blain, H. Planquette
Investigation: S. Blain, I. Obernosterer
Methodology: S. Blain, H. Planquette, A. Guéneuguès
Project Administration: S. Blain
Resources: S. Blain
Validation: S. Blain, H. Planquette
Visualization: S. Blain
Writing – original draft: S. Blain, I. Obernosterer
Writing – review & editing: S. Blain, H. Planquette, I. Obernosterer

Vertical Flux of Trace Elements Associated With Lithogenic and Biogenic Carrier Phases in the Southern Ocean

S. Blain[1], H. Planquette[2], I. Obernosterer[1], and A. Guéneuguès[1]

[1]Sorbonne Université, CNRS, Laboratoire d'océanographie microbienne (LOMIC), Banyuls sur mer, France, [2]CNRS, IRD, Ifremer, LEMAR, University of Brest, Plouzané, France

Abstract Trace elements (TE) are tracers of multiple biotic and abiotic processes in the ocean and some of them are essential for marine life. Vertical export by particles is a major removal process of a large fraction of TE from the surface ocean. However, the seasonal export dynamics and its controlling factors, critical for the understanding of the internal TE cycling, remain poorly constrained. Here, we report and discuss the seasonal export of 15 TE in sinking particles collected by a sediment trap deployed in a highly productive region of the Southern Ocean. Basalt material was the main carrier phase for the export flux of 9 TE, and its dynamic was characterized by a strong decrease over time. TE export driven by biological carriers such as diatom spores and vegetative cells added pulsed seasonal dynamics to the lithogenic signal, while the contribution of fecal pellets was less variable over the season. For each TE, we were able to decipher the biological carrier phases that represent the most dominant export pathway. We discuss this partitioning with regards to the known metabolic functions of the different trace metals or TE of biological interest.

1. Introduction

During the past decade the international project GEOTRACES has undertaken an unprecedented effort to improve our knowledge of the distribution and biogeochemical cycles of trace elements and their isotopes (TEI) in the ocean (Anderson, 2020). Trace metals are required in many metabolic functions (Sunda, 2012) and as such, biogenic particles that are generated in the upper ocean are one of the main players regulating the internal cycling of so called "bioactive" trace elements (TE). TE are incorporated into particles through biological uptake and/or passive adsorption; they can then be remineralized, desorbed and/or ultimately exported. Particle sinking is one of the mechanisms of downward transport of chemical elements (Boyd et al., 2019). Large biogenic particles such as phytoplankton aggregates or fecal pellets are major vectors in the downward transport of particulate organic carbon (POC), but lithogenic particles can also play a role by ballasting aggregates and reducing remineralization (Lemaitre et al., 2020). Due to their role in the control of atmospheric CO_2 (Antia et al., 2001), carbon vertical export fluxes have been extensively studied, yet TE export fluxes have been considerably less investigated.

Vertical fluxes of particulate TE can be determined in different ways (McDonnell et al., 2015). Among them, moored sediment traps have been used since the 1970s to measure vertical fluxes of sinking material in the ocean. Important characteristics of vertical fluxes were revealed by this approach, but possible biases and limitations were also identified leading to the delivery of best practises (Buesseler et al., 2007). Taking these recommendations into account for deployment of the moorings and their design, moored sediment traps are powerful tools and are quite unique to capture long term variability (months to years) of sinking fluxes including TEs (Conte et al., 2019; Huang & Conte, 2009; Kremling & Streu, 1993; Kuss et al., 2010). In the northern Sargasso Sea, the oceanic flux program (OFP) provides the longest time series for elemental composition of export fluxes at three depths. Data collected between 2000 and 2015 were used to build mean seasonal cycles for 19 elements with a monthly temporal resolution (Conte et al., 2019). Based on the assumption that the elemental composition of the upper continental crust approximated lithogenic material composition in the traps, elemental fluxes were partitioned between different phases (organic matter, carbonates, lithogenic, authigenic). Two components have been identified as main drivers of the seasonal dynamics of the elemental fluxes. One of them was coupled to the seasonal cycle of primary production and surface export. The other one was related to internal processes associated with chemical scavenging and particle aggregation (Conte et al., 2019).

Based on a 13 years time series of elemental flux composition at 2000 m in the North East Atlantic, the mean annual cycles (monthly resolution) of 13 elements were reported (Pullwer & Waniek, 2020). Overall, depending

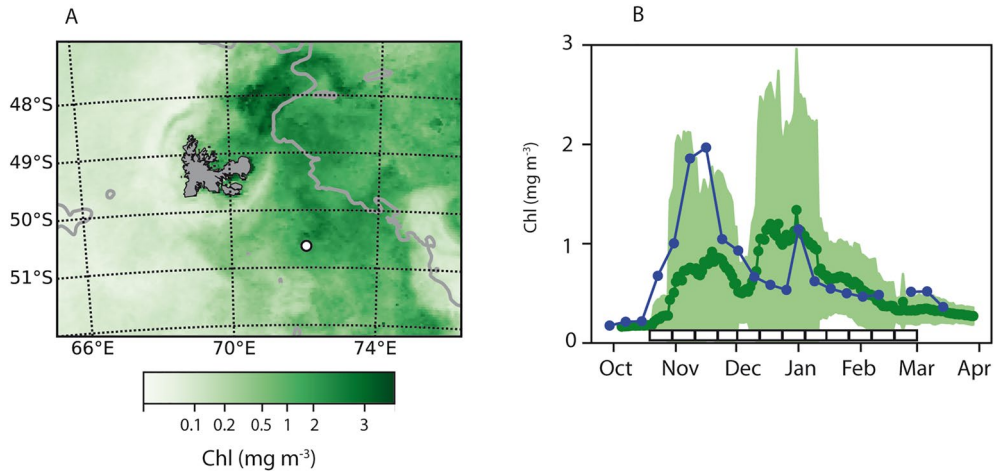

Figure 1. Kerguelen plateau bloom. (a) Monthly composite of chlorophyll surface concentration (mg m^{-3}) for November 2016. The white dot denotes the location of the sediment trap mooring. (b) Seasonal variation of chlorophyll (mg m^{-3}). The blue line corresponds to the 8-day composite chlorophyll concentrations over the season of sediment trap deployment. The green line and light green area represent the climatology and standard deviation respectively. The white rectangles along the *x* axis denote the 12 periods of sediment trap collection.

on the element considered, weak or no seasonality was detected. This was likely due to a small biological signal at the seasonal level, which was further damped by interannual variability of environmental conditions in surface waters. The depth of the traps also likely contributed to mask a clear seasonal signal at this site.

In the Southern Ocean, moored sediment traps were also widely used to investigate carbon export dynamics (Honjo et al., 2000). However, studies of the seasonal dynamics of TE export are rare. The seasonality of particulate export fluxes of 8 TE was studied in the polynya of Pridz Bay (Sun et al., 2016). Seasonal variations of Cu, Zn and Cd were mainly driven by ice coverage and biological production whereas fluxes of Al, Fe and Mn mainly derived from continental debris were controlled by ice melting and freezing processes.

Further investigations of the seasonal export dynamics of TE, with high temporal resolution are therefore required. We have addressed this challenge in the Kerguelen Plateau, a productive region of the Southern Ocean, where iron fertilisation leads to a marked seasonal pattern of carbon export (Blain et al., 2020; Rembauville, Blain, et al., 2015). In this context, we aimed to study and understand the various processes impacting the stoichiometry and the magnitude of these export fluxes, including the seasonal dynamics that can facilitate the partitioning of TE export between different carrier phases.

2. Material and Methods

2.1. Sediment Trap and Sensors

The sediment trap mooring was deployed during the SOCLIM cruise (https://doi.org/10.17600/16003300) on 13 October 2016, at a station located on the central Kerguelen plateau (50°38'344°S, 71°59'854°E) (Figure 1a) in the core of a productive region which is naturally iron fertilized (Blain et al., 2007). The bottom depth is 527 m. Two consecutive diatom blooms occur annually (Blain et al., 2020) with peaks in chlorophyll concentrations within the mixed layer in November and in December (Figure 1b).

We used a Technicap PPS3 sediment trap (0.125 m^2 collecting area, 4.75 aspect ratio) located at 292 m below the surface. The cups were prepared using trace metal clean protocols in a clean room. The cups were washed with warm solution alkalin detergent (Extran) for 24 hr, rinsed 3 times with distilled water, then soaked in 2M HCl (analytical grade) for 1 week, rinsed 3 times with MQ water, soaked in 0.2 M HCl (ultrapure) for 1 week and finally rinsed 3 times with MQ water. The cups were then stored in plastic bags until used. Following the protocol of the preparation of the trace metal clean AQUIL medium (Price et al., 1989), the hypersaline formalin solution buffered at pH = 8 with sodium tetraborate was passed through a Chelex resin to remove trace metal contamination. Trace metal concentrations of this solution can be found in Table S2 in Supporting Information S1. Just prior

Table 1
Sampling Dates for Sediment Trap

Cup number	Opening date	Closing date
1	20/10/2016	01/11/2016
2	01/11/2016	12/11/2016
3	12/11/2016	23/11/2016
4	23/11/2016	04/12/2016
5	04/12/2016	15/12/2016
6	15/12/2016	26/12/2016
7	26/12/2016	06/01/2017
8	06/01/2017	17/01/2017
9	17/01/2017	28/01/2017
10	28/01/2017	08/02/2017
11	08/02/2017	19/02/2017
12	19/02/2017	01/03/2017

to the deployment, the 12 cups (250 mL) were filled with the 5% preservative solution and mounted on the sediment trap carousel. The collection time for each cup was 11 days (Table 1). A current meter (Aquadopp) and an inclinometer were attached to the sediment trap to record measurements of current speeds and inclination of the trap at a frequency of 1 hr^{-1}.

After recovering the sediment traps on 3 April 2017, 1 mL of the supernatant of the cups was immediately replaced by fresh hypersaline formalin buffered (pH = 8) solution before storage at room temperature until further processing. Four months later, at the home laboratory, samples were first transferred to a Petri dish and examined under a stereomicroscope (Leica MZ8, x10 to x50 magnification) to remove swimmers (i.e., organisms for which the structure was well preserved and that actively entered the cup). Then the samples were split into eight aliquots using a Jencons peristaltic splitter (Rembauville, Blain, et al., 2015).

2.2. Bulk Chemical Analysis

Aliquots for chemical analyses were centrifuged for 5 min at 3000 rpm. After this step, the supernatant was withdrawn and replaced by Milli-Q-grade water to remove salts.

This rinsing step was repeated three times. The remaining pellet was freeze-dried (SGD-SERAIL, 0.05–0.1 mbar, −30 to 30°C, 48 hr run) and weighed three times (Sartorius MC 210 P balance, precision of 10^{-4} g) to calculate the total mass. The particulate material was then ground to a fine powder and used for further elemental analysis.

2.2.1. Mass, Total POC/PON, BSi, $CaCO_3$

For particulate organic carbon (POC) and particulate organic nitrogen (PON) analyses, 3–5 mg of the freeze-dried powder was weighed directly into pre-combusted (450°C, 24 hr) silver cups. Samples were decarbonated by adding 20 µL of 2M analytical-grade HCl (Sigma-Aldrich). Samples were dried overnight at 50°C. POC and PON were measured with a CHN analyzer (Perkin Elmer 2400 Series II CHNS/O elemental analyzer) calibrated with glycine. Samples were analyzed in triplicate with an analytical precision of less than 0.7%.

For BSi analysis, 2–8 mg of material was used. For BSi sample digestion we followed the protocol from (Ragueneau et al., 2005) and the silicic acid concentrations in the solutions were determined manually following Aminot and Kérouel (2007). The precision of BSi measurement was 10% (Ragueneau et al., 2005).

For bulk $CaCO_3$ analyses, 5 mg of freeze-dried material was weighed into Teflon vials for the mineralization. One mL of 65% (v/v) HNO_3 (Sigma analytical grade) was added and samples were placed in an ultrasonication bath for 20 min. Samples were then dried overnight at 130°C, then 0.5 mL of 40% (v/v) HF (Sigma analytical grade) and 5 mL of 65% HNO_3 were added. The samples were ultra-sonicated a second time and dried overnight. The resulting residue was dissolved in 10 mL of 0.1 N HNO_3 and the calcium (Ca) content was analyzed by inductively coupled plasma – optical emission spectrometry (ICP-OES, Perkin-ElmerOptima2000). The efficiency of the mineralization procedure was estimated using the reference material GBW-07314. The efficiency was 96% and the precision of the Ca measurement was 2% (Rembauville et al., 2016). Based on a Ca/Ti ratio in basalt of Kerguelen (3.3 mol/mol) we estimate that the contribution of Ca of lithogenic origin to the total Ca flux was low. We therefore equaled the Ca flux to the biological $CaCO_3$ flux.

2.2.2. Elemental Analysis by SF-ICP-MS

For elemental analysis by SF-ICP-MS, between 12 and 40 mg of dried material were transferred into clean PFA vials and were digested in a mixture of 8.0 M HNO_3 (Merck ultrapur) and 2.9 M HF (Merck suprapur). Vials were tightly capped and heated to 130°C for 4 hr. The remaining solution was then evaporated to near dryness, then 400 µL of concentrated HNO_3 (Merck ultrapur) was added to drive off the fluorides and was then evaporated.

Finally, samples were redissolved with 3 mL of 3% HNO_3 (Merck Ultrapur) and kept in acid-cleaned 15 mL polypropylene tubes (Corning®) until analysis by SF-ICP-MS (see details below). This procedure has been proven adequate for digestion of all particulate trace metals (Planquette & Sherrell, 2012).

All archive solutions were analyzed by SF-ICP-MS (Element XR) following the method of Planquette and Sherrell (2012). Final concentrations of samples and procedural blanks were calculated from In-normalized data. Analytical precision was assessed through replicate samples (every 10th sample) and accuracy was deduced from analysis of Certified Reference Materials (CRMs) of plankton (BCR-414) and sediments (PACS-3 and MESS-4) (Table S1 in Supporting Information S1). Dissolved Mn, Fe, Cu, and Co concentrations of the saline solution were determined before deployment and after the recovery in an aliquot collected after the centrifugation, by SF-ICP-MS after preconcentration using the SeaFast (Table S2 in Supporting Information S1) following the method described previously (Tonnard et al., 2020). Based on these results we calculated the percentage of dissolution of the particulate material within the cups (Table S2 in Supporting Information S1). We did not correct particulate flux for dissolution as the values are generally low (<10%) with the exception of Mn (23.5%) in cup #11 and Cu in cups #7 (11.4%), #8 (10.1%) and #11 (30.8%).

2.3. Carbon Export Fluxes of Diatoms and Faecal Pellets

Microscopic observations were conducted within four months after recovery of the moorings. For the identification of diatoms, counting and size measurements, we followed the protocol described in Rembauville, Blain, et al. (2015) that allows the separate consideration of full and empty cells. For diatom counting, the samples were processed as follows. Two mL of one-eighth aliquot was diluted with 18 mL of artificial seawater and decanted in a Sedgewick Rafter counting chamber. Full diatoms were enumerated and identified under an inverted microscope with phase contrast (Olympus IX170) at 400x magnification. The morphometric measurements were done using high resolution images (Olympus DP71 camera) and Fiji image processing software. The biovolume was calculated from morphometric measurements (Hillebrand et al., 1999).

The export flux of diatoms (Cell m^{-2} d^{-1}) was calculated using the equation:

$$Cell\ flux = N_{diat} \times d \times 8 \times V_{aliquot} \times \frac{1}{0.125} \times \frac{1}{11} \times k \quad (1)$$

Where N_{diat} (cell mL^{-1}) is the number of cells counted in one chamber, d is the dilution factor, 8 relates to measurements being made on a one eighth aliquot of the sample, $V_{aliquot}$ (mL) is the volume of the aliquot, 1/0.125 relates to the trap surface area (in m^2), 1/11 relates to the sample collection time (in days), and k is the fraction of the chamber counted.

The diatom flux was then converted to POC flux for each taxon using allometric equations reported in the literature (Cornet-Barthau et al., 2007; Menden-Deuer & Lessard, 2000) and taking into account specific relationships for spores (Rembauville, Blain, et al., 2015) (Table S3 in Supporting Information S1). The spore and vegetative cell carbon fluxes were then obtained by summing up the contribution of the different taxa. The sum of both fluxes corresponded to the carbon flux associated with diatoms.

To enumerate fecal pellets, an entire one-eighth aliquot of each sample cup was placed in a gridded Petri dish and observed under a stereomicroscope (Zeiss Discovery V20) coupled to a camera (Zeiss Axiocam ERc5s) at 10X magnification. Fecal pellets were classified into three types according to their shape: spherical, cylindrical, ovoid/ellipsoid (Table S3 in Supporting Information S1) (Gleiber et al., 2012). Size measurements were used to calculate the volume of each fecal pellet according to their shape that was then converted to carbon using a factor of 0.036 mg C mm^{-3} (González & Smetacek, 1994). The fecal pellets carbon fluxes (F_{fp} (mg C m^{-2} d^{-1})) in the different size classes were calculated using the equation:

$$F_{fp} = C_{fp} \times 8 \times \frac{1}{0.125} \times \frac{1}{11} \quad (2)$$

where C_{fp} (mg C per fecal pellets for each type) is the concentration of carbon in each fecal pellet type. Others terms in the equation have the same definition as in Equation 1). The F_{fp} were finally summed to provide the total fecal carbon fluxes. Although the calculation of total POC flux is associated with large uncertainties (around

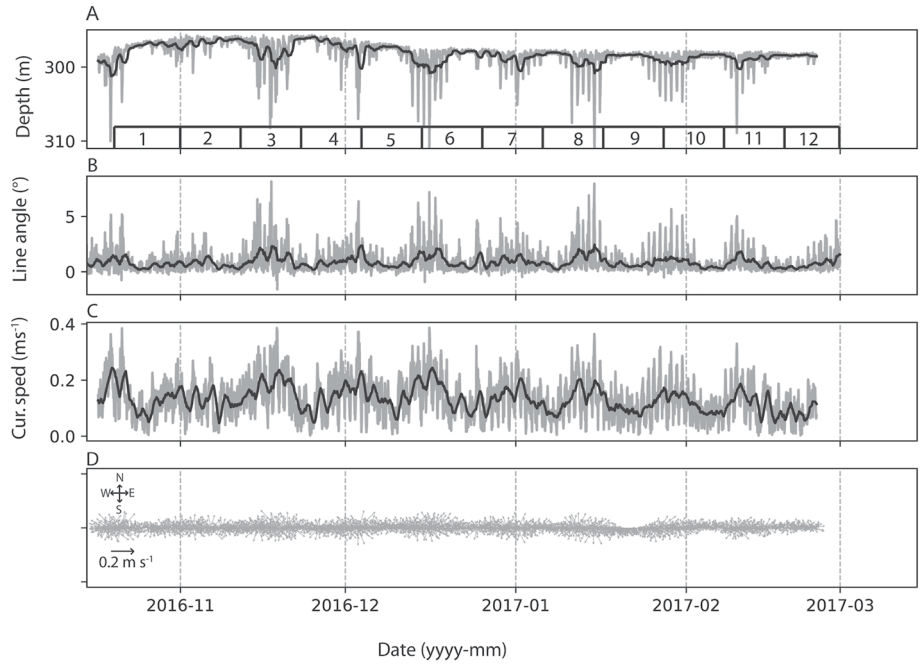

Figure 2. Physical environment of the sediment trap. For all panels, the gray line shows the raw data acquired every 30 min. The black line denotes the running average with a time window of 26 hr. (a) depth of the sediment trap, (b) Inclination angle of the sediment trap (vertical reference = 0°), (c) current speed measured 3 m below the sediment trap. (d) Current direction and intensity.

50%, (Rembauville, Blain, et al., 2015), the linear regression between $POC_{calculated}$ and $POC_{measured}$ was as follows: $POC_{calculated} = (0.84 \pm 0.05)\,x\,POC_{measured} + (0.2 \pm 0.35)$ with $R^2 = 0.9621$.

2.4. Statistics Tools and Data Visualization

Statistical analysis (cross-correlation, Principal Component Analysis (PCA) and Partial least Square Regression (PLSR)) were performed using scikit-learn packages python 2.7. Scipy.stats package python 2.7 was used to conduct ANOVA after checking for homoscedasticity with a levene test. Data visualization was realised with python 2.7 matplot library.

3. Results

3.1. Physical Conditions at the Depth of the Sediment Trap

The average depth of the sediment trap was 293 ± 2 m ($n = 3152$) with a few short and episodic deepening events below 300 m (Figure 2a). The mean inclination angle of the sediment trap was 0.8° ± 1° (Figure 2b). Inclination angles above 2° were rare and associated with deepening events of the trap and current speeds exceeding 0.2 m s^{-1}. The mean current speed was 0.13 ± 0.07 m s^{-1}. The short-term variability of current speed and direction (Figures 2c and 2d) was driven by tide (see Rembauville, Salter, et al., 2015) for a detailed study at the same site and depth and a window of 26 hr is adequate for filtering this short-term variability.

3.2. Seasonal Changes of Mass Flux and Biological Export

The seasonal variations of export fluxes were determined for particle mass, total POC and PON, for $CaCO_3$ and BSi. POC was further partitioned between different biological carrier phases: total diatoms (POC_{diat}), separated into diatom spores (POC_{spore}) and diatom vegetative cells (POC_{veg}), and fecal pellets (POC_{fp}) (Figure 3). Seasonal variations of particle mass, POC, POC_{diat}, and BSi fluxes were characterized by two peaks of export. The first

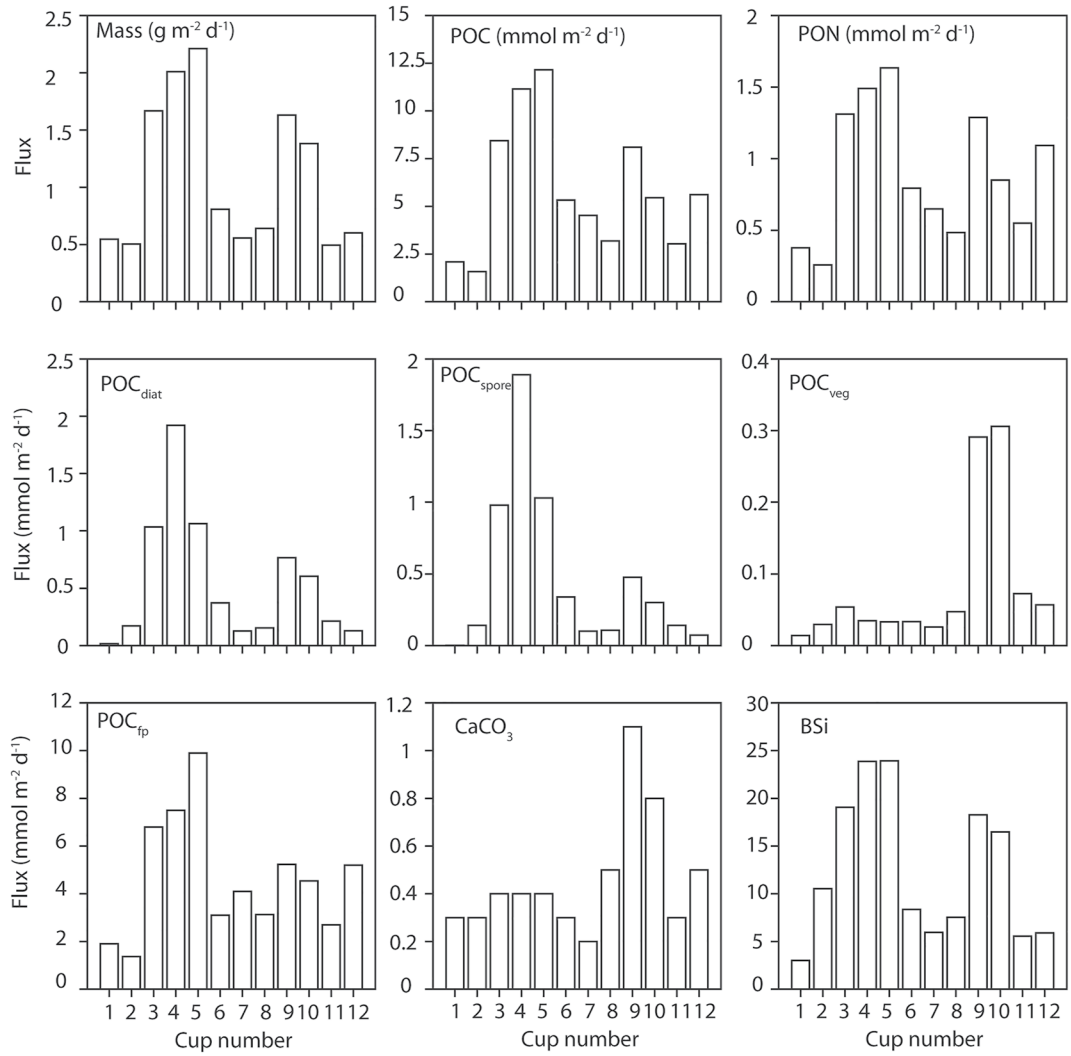

Figure 3. Export fluxes of biological vectors. Each panel shows the seasonal variations of the export flux of the parameter indicated in the upper left corner. Within each panel, vertical bars represent the export fluxes determined in the 12 cups. POC_{diat} is the flux associated with diatoms, POC_{spore} is the flux associated with diatom spores, POC_{veg} is flux associated with diatom vegetative cells and POC_{fp} is the flux associated with fecal pellets.

export event occurred between 12 Nov 2016 and 15 Dec 2016 and was recorded in cups #3 to #5. A second export event occurred between 17 Jan 2017 and 08 Feb 2017 and was recorded in cups #9 and #10. The export of POC_{spore} took place largely during the first event, while POC_{veg} and $CaCO_3$ exports were mainly observed during the second event. High export fluxes of POC_{fp} were also observed during these two main events (cups #4, #5 and #9). On a seasonal basis, the POC export was largely dominated by fecal pellets (89%) while the relative contribution of diatoms (vegetative cells and spores) to total POC never exceeded 11%.

To better understand the seasonal variability of the export via different biological carrier phases we used principal component analysis (PCA) (Figure 4). The first two principal components (PC) explained respectively 72.1% and 20.8% of the total variance. The first PC separated the cups in two categories. Positive values of PC1 correspond to cups with material collected during both major export events (#3, #4, #5 and #9, #10), and negative values of PC1 were related to the other cups. The highly correlated variables (mass, BSi, POC, PON, POC_{fp}, POC_{diat} and POC_{spore}) (Figure S1 in Supporting Information S1) mainly contribute to PC1. The second component (PC2) separated mainly the first (negative values, #3, #4, #5) from the second export event (positive values, #9, #10). The variables contributing mainly to PC2 are POC_{spore} associated with the first export event and POC_{veg} and $CaCO_3$ associated with the second export event.

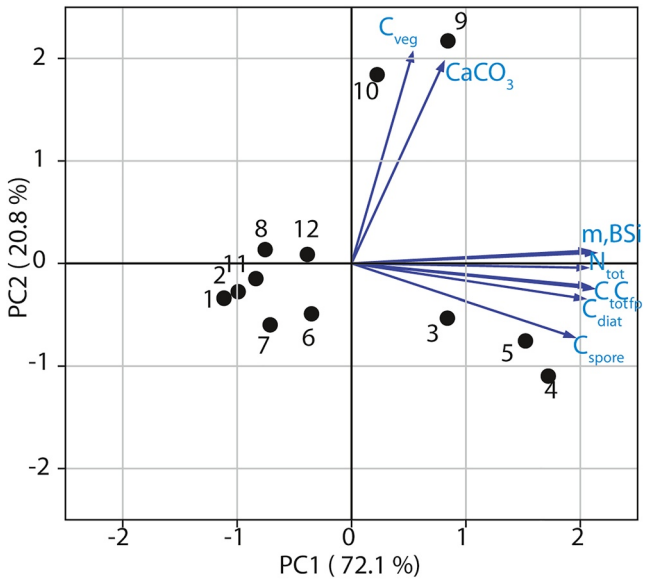

Figure 4. PCA correlation biplots of biological fluxes. Black dots denote the cups associated with their labels from 1 to 12 (1 corresponds to the first cup collected). Blue arrows represent the projection of the descriptors into the two first principal component plan (for clarity their lengths were multiplied by 2). The definition of arrow labels are C_{tot} (flux of total POC), N_{tot} (flux of total PON), C_{veg} (flux of POC associated with vegetative diatoms), C_{spore} (flux of POC from diatom spores), C_{fp} (flux of POC from fecal pellets), $CaCO_3$ (flux of $CaCO_3$), m (flux of total particle mass) and BSi (flux of biogenic silica).

3.3. Seasonal Changes of TE Export

The 12 TE fluxes varied by almost 7 orders of magnitude (Figure 5). The highest flux was recorded for Al with a maximum of 160 μmol m^{-2} d^{-1} and the lowest for Th with a minimum of 3.5×10^{-2} nmol m^{-2} d^{-1}. Examination of the seasonal changes revealed two qualitatively different temporal patterns. High export fluxes of P, Cd, Ba, Mo, Cu, Ni and V were associated with one or both of the main export events described in the previous section. For most of these elements, the export fluxes were higher during the first than during the second event, but more subtle differences appear. For example, the flux of Cd export was much more pronounced during the first than the second event, whereas for V the fluxes were almost identical during both events. For the other elements (Y, Mn, Zr, Co, Ti, Cr, Th, Fe and Al) the highest fluxes were measured in the first cups (#1 to #5) and the lowest in the remaining cups (#6 to #12).

For TE fluxes, a PCA confirms the partitioning between the two main groups mentioned in the previous section based on the qualitative analysis of the seasonal changes (Figure 6). The two first components of the PCA explain 98.2% of the seasonal variation of the TE export. For PC1, positive scores correspond to the beginning of the season (#1 to #5) and negative scores to the remaining cups (#6 to #12). The highest positive scores for the PC2 are typical of cups corresponding to the two export events (#4 #5 and #9 #10). Within the group of elements characterized by two marked peaks of export (P, Cd, Ba, Mo, Cu, Ni and V), the PCA shows three possible subgroups where seasonal variations of these elements are highly correlated. These consist of P, Cd and Ba, then Mo and Cu, and finally Ni and V (Figure S2 in Supporting Information S1).

4. Discussion

Our parallel observations of the seasonal changes in the export fluxes of different biological carrier phases, as defined hereafter, and of trace metals, provide the opportunity to identify the the main factors that control their export in this iron fertilized region of the Southern Ocean.

The bulk composition of particles is usually partitioned between different pools identified as particulate organic matter (POM), biogenic silica (BSi), calcium carbonate ($CaCO_3$), lithogenic and authigenic material (Lam et al., 2015). The partitioning of TEs between these different pools relies on two main hypotheses. First, one assumes that it is possible to identify a chemical element or a chemical form of the element that largely dominates one of the pools and has a minor contribution to the others. For the lithogenic fraction, Al has been extensively used, although Ti has recently gained interest in this context when the potential source material and its chemical composition are clearly identified. For the POM fraction, beside POC that is widely used, phosphorus (P) is also selected as the reference element, because it is a major contributor and has a mineral form (e.g., apathite) with low abundance in seawater. In addition, P is measured simultaneously with metals by analytical methods like Sector Field Induced Coupled Plasma Mass Spectrometry (SF-ICP-MS) or X-ray Fluorescence (XRF) synchrotron (Twining et al., 2003).

The second assumption is that for any given element, the ratio with the reference element of a given fraction must be known or postulated. For the lithogenic pool, the elemental composition of a representative material can be used in order to determine enrichment factors. These enrichment factors provide information on the extent to which TE are associated with particles of lithogenic origin. In most studies, global crustal composition or upper crustal compositions (Taylor & McLennan, 1995) are used, but the composition of local mineral sources like desert dust are also valuable (Kremling & Streu, 1993). For the biogenic fractions, $CaCO_3$ and BSi determinations are straightforward, but there are few experimental data to constrain the ratio of a given TE to $CaCO_3$ (TE/$CaCO_3$) and BSi (TE/BSi) and therefore to derive directly the amount of metal transported by these fractions. The issue is even more complicated for POM due to the diverse composition of this fraction. When POM is

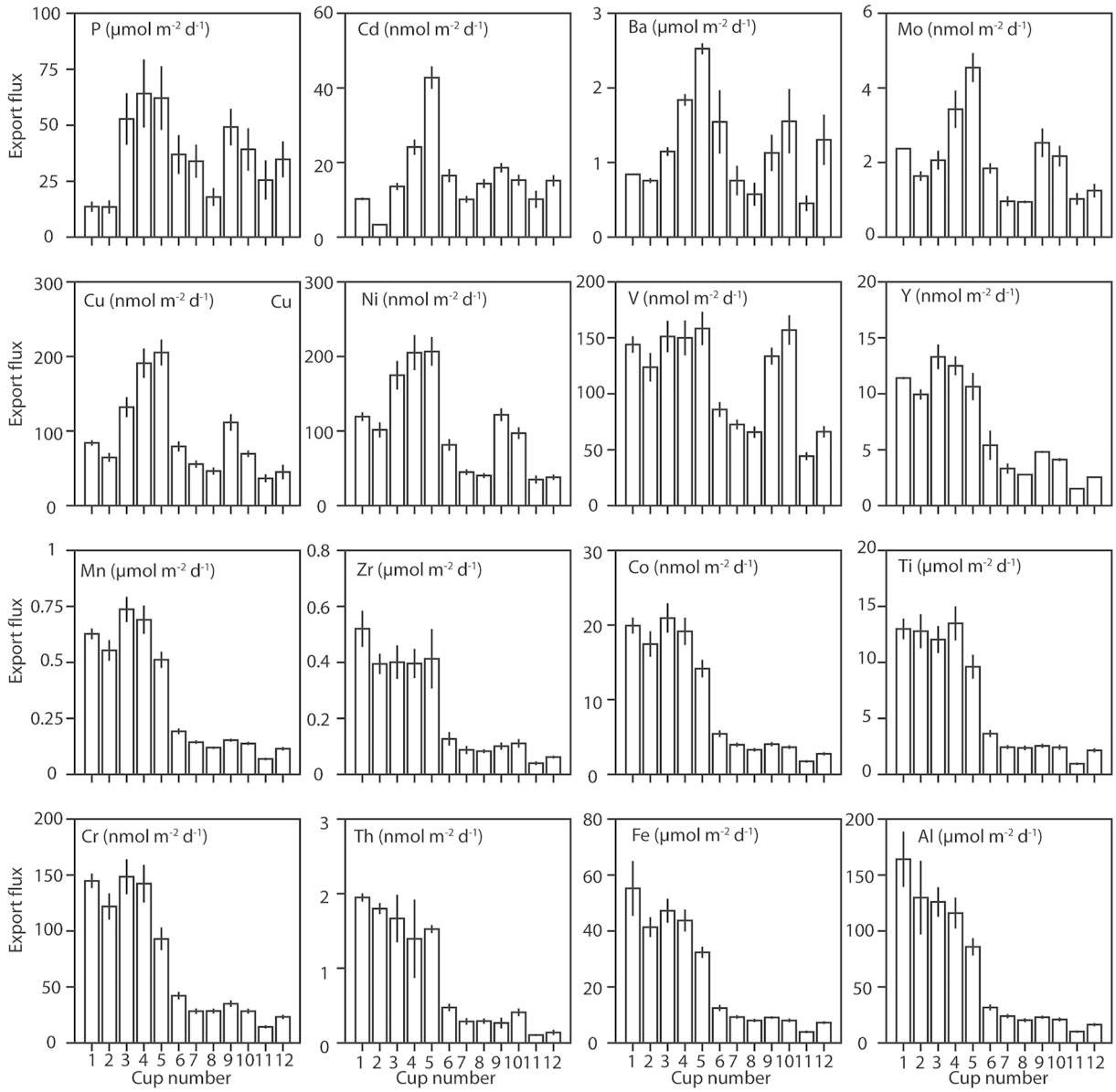

Figure 5. Export fluxes of phosphorus and 11 trace elements. Each individual panel shows the seasonal variability of the export flux of the element with its unit indicated in the left upper corner. Within each panel, vertical bars represent the export fluxes collected in the 12 cups and the vertical lines show the standard deviation based of analytical precision.

dominated by phytoplankton, an extension of the Redfield ratio to metals can be considered, but there are large uncertainties in the determination of phytoplankton TE/P ratios (Twining & Baines, 2013). Moreover, elemental ratios of dead microorganisms can largely differ from those measured in living cells due to the dissolution and remineralization rates that vary between elements. Consequently, TE/P ratios in two important vectors of TE export, phytoplankton aggregates (Twining et al., 2015) or fecal pellets (Fowler, 1977) cannot easily be inferred. For example, different types of particulate organic matter (Lam et al., 2015) could influence surface adsorption of TEs (Balistrieri et al., 1981) and ultimately the TE stoichiometry. Together, these considerations result in a complex dynamic of TEs hosted in dissolved and particulate pools. This is further complicated by the fact that the magnitude of external sources and individual processes are subjected to strong variations throughout the year (Hayes et al., 2015; Sternberg et al., 2007).

In the following, we will discuss our findings from several points of view. First, we will use an approach classically found in the literature and summarized above that provides an estimate of the lithogenic contribution to

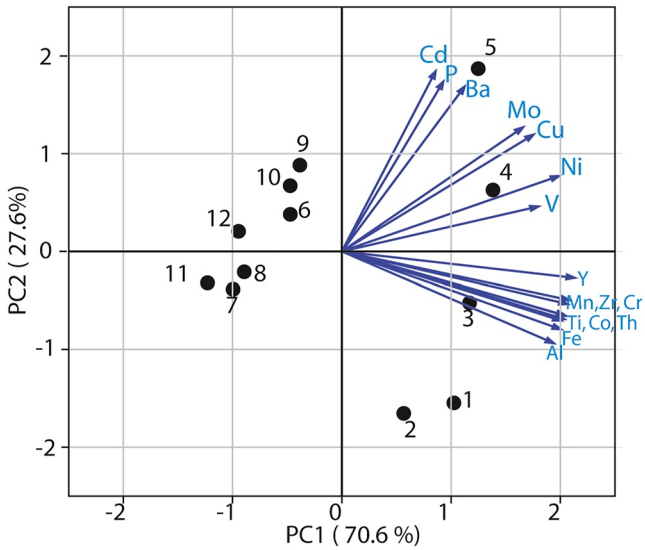

Figure 6. PCA correlation biplots of trace elements: Black dots denote the cups associated with their labels from 1 to 12 (1 corresponds to the first cup collected). Blue arrows represent the projection of the descriptors into the two first principal component plan (for clarity their lengths were multiplied by 2).

Table 2
TE/Ti Ratio

	Upper CC[a]	Basalt [b]i	cups#1–12 [c]	cups#1–2[d]
	TE/Ti	TE/T	TE/Ti	TE/Ti
TE	(g/g)	(g/g)	(g/g)	(g/g)
Ti	1	1	1	1
Al*	26.7	4.2 ± 1.6	5.3 ± 0.7	6.4
Fe*	11.7	5.0 ± 1.7	4.2 ± 0.7	4.4
Mn	0.2	(8.6 ± 2.4) 10^{-2}	(6.3 ± 0.8) 10^{-2}	5.2 10^{-2}
P	0.23	(2.5 ± 1.0) 10^{-5}	6.9 ± 4.9	0.68
Ba	0.18	(1.6 ± 0.9) 10^{-3}	0.9 ± 0.6	0.18
V	2 10^{-2}	(1.4 ± 0.3) 10^{-2}	(2.9 ± 1.8) 10^{-2}	1.1 10^{-2}
Cr*	1.2 10^{-2}	(0.7 ± 1.4) 10^{-2}	(1.2 ± 0.2) 10^{-2}	1.1 10^{-2}
Co*	3.3 10^{-3}	(2.4 ± 1.2) 10^{-3}	(1.8 ± 0.2) 10^{-3}	1.7 10^{-3}
Ni	6.6 10^{-3}	(4.9 ± 7.8) 10^{-3}	(2.7 ± 1.5) 10^{-2}	1.1 10^{-2}
Y*	7.3 10^{-3}	(1.8 ± 0.6) 10^{-3}	(2.3 ± 0.6) 10^{-3}	1.5 10^{-3}
Zr*	6.3 10^{-2}	(1.4 ± 0.7) 10^{-2}	(6.9 ± 1.0) 10^{-2}	6.8 10^{-2}
Th	3.5 10^{-3}	(1.7 ± 1.2) 10^{-4}	(5.8 ± 1.2) 10^{-5}	7.0 10^{-4}

Note. In the first column, the asterisk associated with a given trace element indicates that the mean TE/Ti in Kerguelen basalt and in sediment trap matter is not statistically different ($p = 0.01$).

[a]mean elemental ratios in continental crust (CC) from (Taylor & McLennan, 1995). [b]Mean elemental ratios derived from composition of basalt rocks of Kerguelen island (Weis et al., 1993; Yang et al., 1998). [c]Mean elemental ratios considering all cups. [d]Ratio elemental ratios considering the two first cups.

the TE flux. This approach allows the derivation of the flux not supported by lithogenic carriers which can approximate the biological, scavenged, and authigenic contributions. Second, we will consider simultaneously several possible carrier phases to extract the ones most probably associated with the individual elements. This second approach will be used to investigate further the role of different biological carriers. We will confront these results with recent findings on the biological role of TE in both autotrophic and heterotrophic microorganisms, as revealed by laboratory or in situ omics-based studies.

4.1. Basalt Is the Main Lithogenic Carrier Phase

Using the results of the PCA for TE (Figure 6), we show that Y, Mn, Cr, Ti, Co, Th, Fe, Al and Zr have a similar seasonal export pattern. Some of these elements are well known as representatives of lithogenic matter (i.e., Ti, Cr, Zr, Y, Th and Al), while others like Mn, Co and Fe are also involved in biological processes. The quantitative estimate of the lithogenic fraction of the fluxes relies on both the choice of a reference element and a reference material of a known elemental composition. Al and Ti have been both used previously as reference elements. In the present study we will not use Al because it is known to be associated with diatom frustules (Ren et al., 2013) and a previous study above the Kerguelen plateau has shown that diatoms dominate during spring and summer (Blain et al., 2020). Therefore, Al is likely present in diatoms exported directly via aggregates or indirectly via fecal pellets. Using Al as the reference could therefore lead to an overestimation of the lithogenic fraction, while Ti can provide a more conservative estimate. We thus consider Ti as a reference element for the lithogenic fraction (Ohnemus & Lam, 2014) and calculated the mass ratios F_{TE}/F_{Ti} where F_{TE} is the export flux of a given TE and F_{Ti} is the export flux of Ti collected in the same cup (Table 2).

The choice of the elemental ratio is also critical for the calculation of the lithogenic contribution to TE export fluxes. In the present study, for most of the elements associated mainly with a lithogenic carrier phase, Al, Fe, Cr, Co, Y, Zr, (Figure 6) the TE/Ti ratios (Table 2) are not significantly different ($p = 0.01$) from the composition of basalt rocks collected around the Kerguelen plateau and islands (Kerguelen archipelago, Heard and Mac Donald Islands) (Weis et al., 1993; Yang et al., 1998). However, with the exception of Cr and Y, the TE/Ti ratios measured in the sediment trap differed largely from that typical of upper continental crust (UCC) (Taylor & McLennan, 1995) (Table 2). Yet, the large differences for Fe/Ti and Al/Ti ratios resulted very likely from the high Ti content of island basalt (Prytulak & Elliott, 2007). We also note that the Mn/Ti ratios are not significantly different from Kerguelen basalt, if a few basalt samples with low Ti (ratio < 2) are excluded from this analysis. Therefore, derived basalt particles are likely the main contributors to the lithogenic export fluxes, although alteration of rocks and subsequent transformation during transport in terrestrial and marine environments could modify the chemical composition of lithogenic particles.

We calculated for individual elements the average TE/Ti based on: (a) all cups and (b) only the first two cups and compared with the TE/Ti ratios in the UCC and in the Kerguelen basalt (Table 2). We then estimated the lithogenic contribution to TE export fluxes using Equation 3:

$$F_{TElith} = (TE/Ti) \times F_{Ti} \quad (3)$$

where TE/Ti is the average ratio for the two first cups. In Figure 4, the projection of cups #1 and #2 presented the most negative score along PC1 suggesting that TE export fluxes collected in this trap were mainly driven by non-biological carriers. Moreover, the PCA of TE export fluxes (Figure 6) shows that the projections of cups#1 and #2 were located in the quarter of space that was related to a suite of TEs typically associated with basalt. This analysis of both PCAs clearly identify these cups as mainly associated with lithogenic material and suggests they are therefore the most appropriate to estimate a lithogenic elemental ratio for the sediment trap material. We note that including cups #3, #4 and #5 in the calculation of the individual elemental ratio would have resulted in a biased estimate due to the contribution of biological fluxes. We also calculated the residual export flux, which is not associated with lithogenic material for each element using Equation 4:

$$F_{xs} = F_{TE} - F_{TElith} \quad (4)$$

and these residual fluxes are represented on Figure 7.

Our observations clearly underscore that the residual export fluxes of 6 elements (Zr, Co, Cr, Th, Fe, Al) estimated using this ratio are occasionally or consistently negative throughout the season (Figure 7). Regarding Fe, the order of magnitude of an expected biogenic flux based on the export flux of P (P_{xs}) can be estimated. Considering the highest values of P_{xs} of 50 µmol m^{-2} d^{-1} in cup#5, and using a high estimate for the Fe quota (Fe:P = 5 mmol mol^{-1} (Twining & Baines, 2013)), one would expect 0.25 µmol m^{-2} d^{-1} of biogenic Fe at the time of the peak flux. This represents around 0.5% of the total flux of Fe measured (Figure 5), confirming that such low contributions cannot be detected using the calculation of the residual fluxes (Fe_{xs} Equation 4). This result, together with the negative values of residual export fluxes, highlight that any contribution of a carrier phase (e.g., biological) other than basalt derived particles cannot be detected using this approach.

4.2. Role of Different Biological Carriers in the Export of TE

In the following, we consider the 9 elements (P, Cd, Ba, Mo, Cu, Ni, V, Y, Mn) for which F_{xs} are positive throughout the season (Figure 7). Among these, 7 elements (P, Mo, Cd, Cu, Ni, V, Mn) have known biological functions and can therefore be directly associated with biological carrier phases. Overall, this is confirmed by the seasonal dynamics of their F_{xs} that presented 1 or 2 maxima corresponding to the cups that collected sinking material during the first (cups# 3, 4, 5) or second (cups# 9, 10) export event. To go a step forward, we took advantage of the detailed description of biological matter export provided by microscopic observations (Rembauville, Blain, et al., 2015) in the same cup material. An important aspect was to quantify the carbon content of exported diatoms and all types of fecal pellets. Microscopic observations revealed that diatoms dominated the phytoplankton community (Blain et al., 2020), and that 12 different taxa contributed significantly (>1% of total biomass) to both the surface carbon biomass and carbon export. However, the concentrations of TE with a biological role certainly varied throughout the season in surface waters due to intense uptake and remineralization as observed for Fe above the Kerguelen plateau (Blain et al., 2008; Bowie et al., 2015). Similarly, TE quota are likely to vary over time in surface diatoms, with consequences on TE composition of the fecal pellets. The absence of data on seasonal changes in TE concentrations in the water column and the large uncertainty of the TE transfer efficiency between phytoplankton and zooplankton led us to make a rather conservative choice of only three biological carriers, vegetative cells, spores and fecal pellets. Additionally, we considered the total particle mass, POC, PON, POC_{diat}, and used $CaCO_3$ as a tracer of calcifying organisms.

We first investigated the role of these different biological carriers using PCA (Figure S3 in Supporting Information S1) based on F_{xs} and the different biological carriers mentioned above. However, this approach did not prove informative on the association of a given TE with a biological carrier, except for V, which was strongly associated with vegetative cells and/or calcifying organisms exported during the second bloom. The strong association of Mn with the first bloom, as revealed by the PCA, is not meaningful, because F_{xs} of Mn is high only in cup #3 albeit the export of this bloom is collected by cups #4 and #5 as well (Blain et al., 2020). For Ba and Y, the PCA does not provide any clues on their association with a particular biological carrier. Co-linearity between the different biological descriptors may have hampered the emergence of more significant relationships for other elements.

We have therefore analyzed the data set using a different statistical tool, the Partial Least Square Regression (PLSR), also referred to as Projection of Latent Structure Regression (Abdi, 2010). This method considers a set

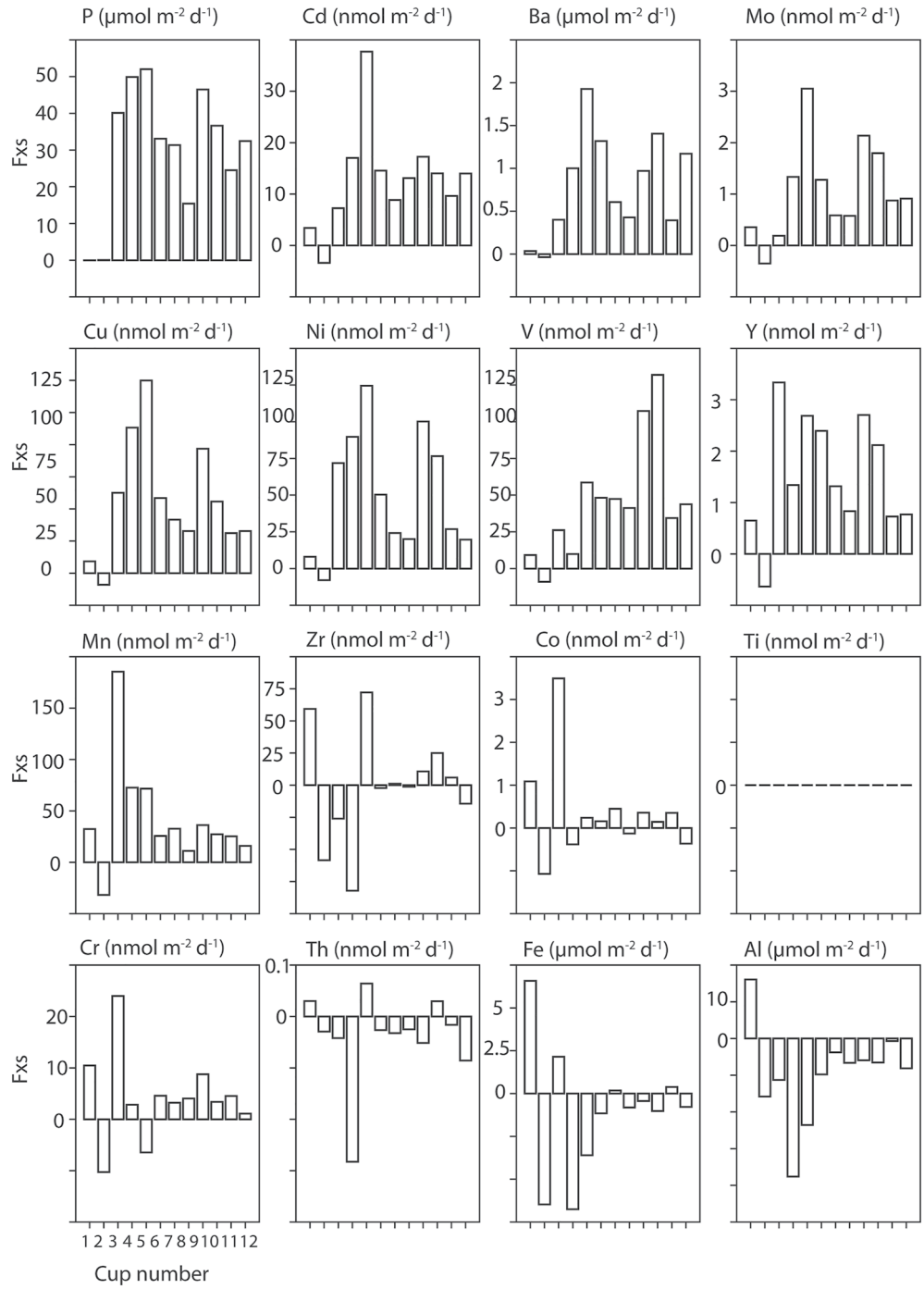

Figure 7. Residual export of trace elements. Each individual panel shows the seasonal variability of the residual export flux F_{xs} (see text for definition) of the element with its unit indicated in the left upper corner.

of predictors (X) and descriptors (Y) and extracts a single set of scores from both simultaneously. The method can be seen as a simultaneous PCA on X and Y which achieves the best relationships between X and Y. The method is efficient even when the variables are possibly correlated and when the number of variables is large compared to the number of observations. This method has been successfully applied to determine the ecological vectors associated with sinking carbon flux (Rembauville, Blain, et al., 2015), to predict the partitioning of carbon within plankton assemblages based on bio-optical properties (Rembauville et al., 2017) or to link biological diversity and carbon fluxes (Guidi et al., 2016). To apply PLSR we considered the total export flux of

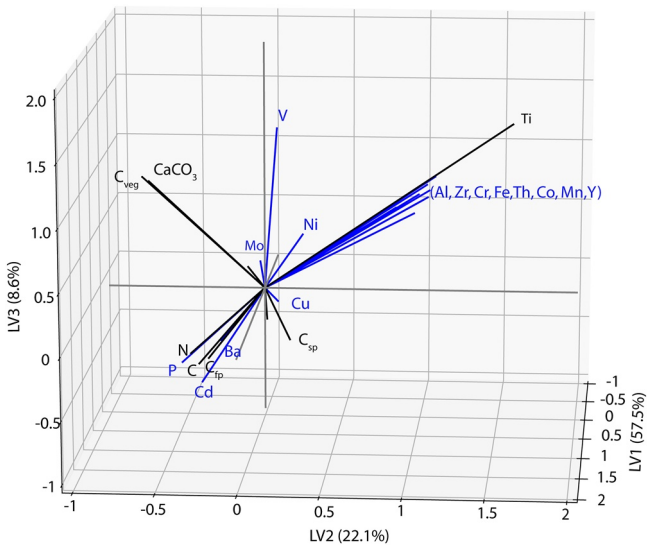

Figure 8. Partitioning of total trace element export fluxes between different carrier phases. The plot presents the projections of both predictors (in black) and descriptors (in blue) in a 3-dimensional space formed by the 3 first latent variables resulting from PLSR analysis which explained 57.5%, 22.1% and 8.6% of the covariance.

the 15 elements (descriptors) and the different biological vectors (predictors) mentioned above, and we considered Ti as an overall predictor of lithogenic material. It is important to note that with this approach the search for relationships between elements and the lithogenic carrier phase does not require the use of an elemental ratio. To summarize the results of the PLSR analysis we present the projections of both descriptors and predictors in a three-dimensional space defined by the three first latent variables (Figure 8) which represent 57.5%, 22.1% and 8.6% of the covariance, respectively. The three corresponding 2D dimensional projections in the latent vectors space are provided in Figure S4 in Supporting information S1. Three different groups of TE emerge from this analysis.

4.2.1. TEs Associated With the Lithogenic Carrier Phase

The PLSR, clearly identifies a group of TEs (Al, Zr, Cr, Fe, Th, Co, Mn and Y) for which the seasonal dynamics are strongly related to the lithogenic carrier phase, represented by Ti. This result is in line with the conclusions of the PCA and TE_{xs} analysis (Figure 6).

4.2.2. TEs Associated With Fecal Pellets and Diatom Spores

The export of Cd, P and Ba was strongly associated with POC_{fp} and to a lesser extend to POC_{sp}. For Ba, this result is not surprising considering that particulate Ba is largely found as authigenic mineral barite in the ocean (Dehairs et al., 1980), formed by precipitation from dissolved Ba in microenvironments where it becomes supersaturated with respect to barite. Such environments are fecal pellets (Alldredge & Cohen, 1987; Ploug, 2001) or aggregates like marine snow which in our study contained large quantities of spores (Blain et al., 2020). Strong correlations of Cd and P export fluxes have already been observed with sediment traps deployed in the upper water column (>1500m) whereas this relationship vanished at greater depth (Conte et al., 2019; Ho et al., 2011). In the present study, the export of Cd was mainly driven by spores during the first bloom and by fecal pellets throughout the season, while vegetative cells and calcifying organisms present during the second bloom played a minor role for Cd export. Cd, but also Co, can substitute for Zn in the carbonic anhydrase (CA) enzyme, Cd-CA and Zn-CA, respectively (Morel et al., 2020). This has been demonstrated for diatoms under low Zn conditions (Lane & Morel, 2000). Cd-CA is present in *Thalassiosira antarctica*, *Chaetoceros dichaeta*, *Proboscia alata* and *Proboscia inermis* (Morel et al., 2020), species that were well represented in our sediment traps (Blain et al., 2020). Interestingly *T. antarctica* and *C. dichatea* are small and spore forming diatoms which dominated during the first bloom, while the genus *Proboscia* contains large diatoms exported as vegetative cells that thrived during the second bloom. Cd utilisation by different diatoms in surface waters could explain the seasonal variation of Cd export in the sediment traps. Cd can also be coincidentally taken up by the divalent transporter under Fe-limited conditions (Horner et al., 2013; Lane et al., 2008). At the beginning of the season, the reservoir of Zn and Fe was large above the Kerguelen plateau (Wang et al., 2019), but the rapid development of the massive bloom of small diatoms could lead to a rapid decrease in Zn to levels at which the substitution of Zn by Cd in CA occurred and/or Cd being taken up by the divalent transporter. No strong signal of particulate Cd was associated with the second bloom suggesting that the substitution of Zn by Cd in CA or divalent transport uptake are not dominant processes at the end of the productive season, either due to increased Zn or Fe concentrations provided by remineralization after the first bloom or due to lower requirements of large diatom cells which do not need Cd for CA activities. Although calcifying organisms including coccolithophorids, present during the second bloom, have high Cd requirements (Ho et al., 2003; Sunda, 2012), their contribution was likely hidden behind the large fluxes associated with fecal pellets.

4.2.3. TEs Associated With Lithogenic and Biological Carrier Phases

V, Mo, Cu and Ni export fluxes are both driven by lithogenic and biological carrier phases. This is a consequence of both their significant contribution to Kerguelen basalt composition (Table 2) and their biological role in microorganisms. Using a similar approach to that used for Cd, we examine the seasonal dynamics of the export of

these four metals by first summarizing a few recent insights on their biological role for microorganisms relevant for our study. We then discuss how these observations can provide clues to understand the seasonal dynamics of their export.

The main non-lithogenic V export event coincided with the flux of large vegetative diatoms and calcifying organisms after the second bloom (Figure 6). Due to the similar seasonal patterns of these biological carrier phases, it is not possible, based on PLSR, to make a clear preferential association with either of them. The current knowledge on the biological role of V is mainly related to diatoms, thus our discussion on the temporal changes of V export focuses on this phytoplankton group. V is a cofactor of haloperoxidase enzymes (VHPO) that produce organo-halogens (Hill & Manley, 2009; Moore et al., 1996; Murphy et al., 2000). Haloperoxidase activity by diatoms could alter the quorum sensing of prokaryotes and therefore protect diatoms against algicidal prokaryotes (Amin et al., 2012). In contrast to the seasonal dynamics of all other elements, the export of V associated to the biological fraction was higher during the second than during the first bloom (Figure 7). Seasonal observations of diatom and prokaryotic communities in the surface layer revealed compositional changes and strong associations (positive and negative) between diatom species and prokaryotic taxa (Liu et al., 2020). Positive associations could result from interactions based on the exchange of metabolites between diatoms and prokaryotes for resource acquisition, but negative associations are more difficult to interpret. The seasonal dynamics of non-lithogenic particulate V, if related to VHPO activity, could suggest that some diatoms efficiently reduce the growth of targeted prokaryotic taxa with algicidal activity in the phycosphere.

The prevalence of non-lithogenic particulate V during the second bloom could be related to seasonal changes of the bioavailability of Fe. Haloperoxidase can contain Fe-heme as prosthetic group instead of V. Fe-heme containing enzymes could dominate the haloperoxidase activity of diatoms when the bioavailable Fe stock is high such as at the beginning of the season. However, as biological uptake during the first bloom consumed a large part of the bioavailable Fe, haloperoxidase activity of diatoms dominating during the second bloom may have switched to VHPO, which requires the uptake of vanadate, an anion that is always present at non-limiting concentrations in seawater. V can also be found in nitrogenase (*nif*) involved in the fixation of dinitrogen (N_2) where it substitutes Mo. A recent study illustrated that Mo/Fe containing *nif* genes are overexpressed by prokaryotic communities on marine particles (Debeljak et al., 2021). Therefore, the association of V or Mo with vegetative diatoms could partly be explained by N_2 fixing prokaryotes attached to particles and their downward transport could be a biological carrier phase for Mo and V.

The dominant biological carrier phase for Cu was different to that of V and Mo. Cu export was mainly related to diatom spores and to a lesser extend to fecal pellets whereas no clear association with vegetative cells and $CaCO_3$ was observed (Figure 8 and Figure S4 in Supporting Information S1). Cu is a co-factor of a large number of oxidative enzymes involved in different metabolic pathways including Fe acquisition (Maldonado & Price, 2001) and nitrogen cycling (Kuypers et al., 2018). Another noticeable feature of these Cu proteins is that most of them are located outside eukaryotic cells or in the periplasm of prokaryotes (Silva and Williams, 2001). A possible consequence can be that Cu enzymes are prone to rapid degradation and release of Cu following cell death. Fecal pellets or spores could provide a protected environment during export, which could explain our observations.

The biological carrier phases for Ni were mainly diatoms (spores or vegetative cells) and fecal pellets had a minor role. Among the many biological pathways, Ni is involved in the assimilation of urea (Oliveira & Antia, 1984) and is also the cofactor of an enzyme of the superoxide dismutase (SOD) family which can substitute for Fe-superoxide dismutase in low Fe environments (Cuvelier et al., 2010; Dupont et al., 2010). These requirements for Ni likely lead to high Ni quota of diatoms relative to other phytoplankton groups (Twining et al., 2012). It was, however, also noted that 50% of Ni contained in diatoms is associated with the frustule with an unknown function. These Ni dependent enzymes suggest that diatom spores, vegetative cells and fecal pellets that contained mainly diatoms are all potential biological vectors of Ni export. If true, the lack of a marked difference between the first and the second bloom dominated by spores and vegetative cells, respectively, is surprising. A larger contribution of diatoms to Ni export would be expected during the second bloom for two reasons. First, the assimilation of urea is likely only noticeable when the switch from NO_3^- to NH_4^+ uptake has occurred, thus after the first bloom. Second, since Fe bioavailability was lower during the second bloom, Fe-SOD is likely to be replaced by Ni-SOD. We suggest an additional process to significantly contribute to the biological export of Ni. Methanogenic *Archaea* utilise different enzymes belonging to the hydrogenase, reductase or CO dehydrogenase families where Ni is present as co-factor (Mulrooney & Hausinger, 2003). Methanogenic *Archaea* have been detected in different

marine particles like marine snow or fecal pellets (Maarel et al., 1999) where they could thrive within anoxic niches (Alldredge & Cohen, 1987; Ploug, 2001). A time series of the composition of the particulate matter in the surface layers would certainly provide new data required to decipher between these different hypotheses.

5. Conclusion

Our observations of the seasonal particulate TE export in a productive region of the Southern Ocean have revealed that the identification of the carrier phases is critical for our understanding of the export dynamics of individual TE. The lithogenic and biological carrier phases identified in our study had distinct temporal patterns. Basalt particles, the main lithogenic carrier phase dominated the export flux early in the season and strongly decreased over time, reflected in the particulate export pattern of TE representative of lithogenic matter (Ti, Cr, Zr, Y, Th and Al) and of TE with a defined biological role (Mn, Co and Fe). The biological carrier phases, diatom vegetative cells and spores, revealed two pulsed export events, while vertical transport *via* fecal pellets remained stable over time. TE with known biological functions (Cd, Ba, Mo, Cu, Ni and V) were associated with one or both of these main export events.

A further look into the seasonal variability of stocks of bioavailable TE is necessary to better understand how these influence the phytoplankton assemblage, inherent enzyme strategies, and subsequent TE utilisation and exports. Finally, future studies should investigate TE composition of individual fecal pellets produced by different zooplankton species feeding on distinct food sources. This could provide insight to help decipher the contribution of each zooplankton species to TE export.

Conflict of Interest

The authors declare no conflicts of interest relevant to this study.

Data Availability Statement

Data are available at the SEANOE database https://www.seanoe.org/data/00606/71768/.

Acknowledgments
We thank the captains and the crew of the R/V Marion Dufresne for their support during the two cruises. We thank E. de Saint Léger, F. Pérault from DT-INSU, and people of IPEV (Institut Polaire Paul Emile Victor) for the technical support during preparation, deployment and recovery of moorings. We thank Nathalie Leblond (Laboratoire Océanographie de Villefranche sur mer) for processing the samples and performing chemical analysis. We thank Mathieu Rembauville for his help during deployment of the clean traps. We thank the anonymous reviewers and the associated editor for their careful reading of the manuscript and for their comments and suggestions that have improved our manuscript. This work is part of the project SOCLIM supported by the Climate Initiative of the foundation BNP Paribas, the French research program LEFE-CYBER of INSU-CNRS, IPEV, Sorbonne Université, and the Flotte Océanographique Française. This work was also supported by the project SEATRAK funded by the French research program LEFE-CYBER.

References

Abdi, H. (2010). Partial least squares regression and projection on latent structure regression (PLS Regression). *Wiley interdisciplinary reviews: computational statistics*, *2*(1), 97–106. https://doi.org/10.1002/wics.51

Alldredge, A. L., & Cohen, Y. (1987). Can microscale chemical patches persist in the sea? Microelectrode study of marine snow, fecal pellets. *Science*, *235*(4789), 689–691. https://doi.org/10.1126/science.235.4789.689

Amin, S. A., Parker, M. S., & Armbrust, E. V. (2012). Interactions between diatoms and bacteria. *Microbiology and Molecular Biology Reviews*, *76*(3), 667–684. https://doi.org/10.1128/MMBR.00007-12

Aminot, A., & Kérouel, R. (2007). *Dosage automatique des nutriments dans les eaux marines: Méthodes en flux continu*. Ifremer.

Anderson, R. F. (2020). Geotraces: Accelerating research on the marine biogeochemical cycles of trace elements and their isotopes. *Annual Review of Marine Science*, *12*(1), 49–85. https://doi.org/10.1146/annurev-marine-010318-095123

Antia, A. N., Koeve, W., Fischer, G., Blanz, T., Schulz-Bull, D., Scholten, J., et al. (2001). Basin-wide particulate carbon flux in the Atlantic Ocean: Regional export patterns and potential for atmospheric CO_2 sequestration. *Global Biogeochemical Cycles*, *15*(4), 845–862. https://doi.org/10.1029/2000GB001376

Balistrieri, L., Brewer, P. G., & Murray, J. W. (1981). Scavenging residence times of trace metals and surface chemistry of sinking particles in the deep ocean. *Deep-Sea Research Part A. Oceanographic Research Papers*, *28*(2), 101–121. https://doi.org/10.1016/0198-0149(81)90085-6

Blain, S., Quéguiner, B., Armand, L., Belviso, S., Bombled, B., Bopp, L., et al. (2007). Effect of natural iron fertilisation on carbon sequestration in the Southern Ocean. *Nature*, *446*(7139), 1070–1075. https://doi.org/10.1038/nature05700

Blain, S., Rembauville, M., Crispi, O., & Obernosterer, I. (2020). Synchronized autonomous sampling reveals coupled pulses of biomass and export of morphologically different diatoms in the Southern Ocean. *Limnology and Oceanography*, *11638*(3), 753–764. https://doi.org/10.1002/lno.11638

Blain, S., Sarthou, G., & Laan, P. (2008). Distribution of dissolved iron during the natural iron-fertilization experiment KEOPS (Kerguelen Plateau, Southern Ocean). *Deep Sea Research Part II: Topical Studies in Oceanography*, *55*(5–7), 594–605. https://doi.org/10.1016/j.dsr2.2007.12.028

Bowie, A. R., van der Merwe, P., Quéroué, F., Trull, T., Fourquez, M., Planchon, F., et al. (2015). Iron budgets for three distinct biogeochemical sites around the Kerguelen Archipelago (Southern Ocean) during the natural fertilisation study, KEOPS-2. *Biogeosciences*, *12*(14), 4421–4445. https://doi.org/10.5194/bg-12-4421-2015

Boyd, P. W., Claustre, H., Levy, M., Siegel, D. A., & Weber, T. (2019). Multi-faceted particle pumps drive carbon sequestration in the ocean. *Nature*, *568*(7752), 327–335. https://doi.org/10.1038/s41586-019-1098-2

Buesseler, K. O., Antia, A. N., Chen, M., Fowler, S. W., Gardner, W. D., Gustafsson, O., et al. (2007). An assessment of the use of sediment traps for estimating upper ocean particle fluxes. *Journal of Marine Research*, *65*(3), 345–416. https://doi.org/10.1357/002224007781567621

Conte, M. H., Carter, A. M., Koweek, D. A., Huang, S., & Weber, J. C. (2019). The elemental composition of the deep particle flux in the Sargasso Sea. *Chemical Geology*, *511*, 279–313. https://doi.org/10.1016/j.chemgeo.2018.11.001

Cornet-Barthau, V., Armand, L., & Quéguiner, B. (2007). Biovolume and biomass estimates of key diatoms in the Southern Ocean. *Aquatic Microbial Ecology*, *48*, 295–308. https://doi.org/10.3354/ame048295

Cuvelier, M. L., Allen, A. E., Monier, A., McCrow, J. P., Messié, M., Tringe, S. G., et al. (2010). Targeted metagenomics and ecology of globally important uncultured eukaryotic phytoplankton. *Proceedings of the national academy of sciences* (Vol. 107, pp. 14679–14684). https://doi.org/10.1073/pnas.1001665107

Debeljak, P., Blain, S., Bowie, A., Merwe, P., Bayer, B., & Obernosterer, I. (2021). Homeostasis drives intense microbial trace metal processing on marine particles. *Limnology & Oceanography*, *66*(10), 3842–3855. https://doi.org/10.1002/lno.11923

Dehairs, F., Chesselet, R., & Jedwab, J. (1980). Discrete suspended particles of barite and the barium cycle in the open ocean. *Earth and Planetary Science Letters*, *49*(2), 528–550. https://doi.org/10.1016/0012-821X(80)90094-1

Dupont, C. L., Buck, K. N., Palenik, B., & Barbeau, K. (2010). Nickel utilization in phytoplankton assemblages from contrasting oceanic regimes. *Deep Sea Research Part I: Oceanographic Research Papers*, *57*(4), 553–566. https://doi.org/10.1016/j.dsr.2009.12.014

Fowler, S. W. (1977). Trace elements in zooplankton particulate products. *Nature*, *269*(5623), 51–53. https://doi.org/10.1038/269051a0

Gleiber, M., Steinberg, D., & Ducklow, H. (2012). Time series of vertical flux of zooplankton fecal pellets on the continental shelf of the Western Antarctic Peninsula. *Marine Ecology Progress Series*, *471*, 23–36. https://doi.org/10.3354/meps10021

González, H., & Smetacek, V. (1994). The possible role of the cyclopoid copepod Oithona in retarding vertical flux of zooplankton faecal material. *Marine Ecology Progress Series*, *113*, 233–246. https://doi.org/10.3354/meps113233

Guidi, L., Chaffron, S., Bittner, L., Eveillard, D., Larhlimi, A., Roux, S., et al. (2016). Plankton networks driving carbon export in the oligotrophic ocean. *Nature*, *532*(7600), 465–470. https://doi.org/10.1038/nature16942

Hayes, C. T., Fitzsimmons, J. N., Boyle, E. A., McGee, D., Anderson, R. F., Weisend, R., & Morton, P. L. (2015). Thorium isotopes tracing the iron cycle at the Hawaii Ocean Time-series Station ALOHA. *Geochimica et Cosmochimica Acta*, *169*, 1–16. https://doi.org/10.1016/j.gca.2015.07.019

Hill, V. L., & Manley, S. L. (2009). Release of reactive bromine and iodine from diatoms and its possible role in halogen transfer in polar and tropical oceans. *Limnology & Oceanography*, *54*(3), 812–822. https://doi.org/10.4319/lo.2009.54.3.0812

Hillebrand, H., Dürselen, C.-D., Kirschtel, D., Pollingher, U., & Zohary, T. (1999). Biovolume calculation for pelagic and benthic microalgae. *Journal of Phycology*, *35*(2), 403–424. https://doi.org/10.1046/j.1529-8817.1999.3520403.x

Ho, T.-Y., Chou, W.-C., Lin, H.-L., & Sheu, D. D. (2011). Trace metal cycling in the deep water of the South China Sea: The composition, sources, and fluxes of sinking particles. *Limnology & Oceanography*, *56*(4), 1225–1243. https://doi.org/10.4319/lo.2011.56.4.1225

Ho, T.-Y., Quigg, A., Finkel, Z. V., Milligan, A. J., Wyman, K., Falkowski, P. G., & Morel, F. M. M. (2003). The elemental composition of some marine phytoplanton. *Journal of Phycology*, *39*(6), 1145–1159. https://doi.org/10.1111/j.0022-3646.2003.03-090.x

Honjo, S., Francois, R., Manganini, S., Dymond, J., & Collier, R. (2000). Particle fluxes to the interior of the Southern Ocean in the Western Pacific sector along 170°W. *Deep Sea Research Part II: Topical Studies in Oceanography*, *47*(15–16), 3521–3548. https://doi.org/10.1016/s0967-0645(00)00077-1

Horner, T. J., Lee, R. B. Y., Henderson, G. M., & Rickaby, R. E. M. (2013). Nonspecific uptake and homeostasis drive the oceanic cadmium cycle. In *Proceedings of the national academy of sciences* (Vol. 110, pp. 2500–2505). https://doi.org/10.1073/pnas.1213857110

Huang, S., & Conte, M. H. (2009). Source/process apportionment of major and trace elements in sinking particles in the Sargasso sea. *Geochimica et Cosmochimica Acta*, *73*(1), 65–90. https://doi.org/10.1016/j.gca.2008.08.023

Kremling, K., & Streu, P. (1993). Saharan dust influenced trace element fluxes in deep North Atlantic subtropical waters. *Deep Sea Research Part I: Oceanographic Research Papers*, *40*(6), 1155–1168. https://doi.org/10.1016/0967-0637(93)90131-L

Kuss, J., Waniek, J. J., Kremling, K., & Schulz-Bull, D. E. (2010). Seasonality of particle-associated trace element fluxes in the deep northeast Atlantic Ocean. *Deep Sea Research Part I: Oceanographic Research Papers*, *57*(6), 785–796. https://doi.org/10.1016/j.dsr.2010.04.002

Kuypers, M. M. M., Marchant, H. K., & Kartal, B. (2018). The microbial nitrogen-cycling network. *Nature Reviews Microbiology*, *16*(5), 263–276. https://doi.org/10.1038/nrmicro.2018.9

Lam, P. J., Ohnemus, D. C., & Auro, M. E. (2015). Size-fractionated major particle composition and concentrations from the US GEOTRACES North Atlantic zonal transect. *Deep Sea Research Part II: Topical Studies in Oceanography*, *116*, 303–320. https://doi.org/10.1016/j.dsr2.2014.11.020

Lane, E. S., Jang, K., Cullen, J. T., & Maldonado, M. T. (2008). The interaction between inorganic iron and cadmium uptake in the marine diatom Thalassiosira oceanica. *Limnology & Oceanography*, *53*(5), 1784–1789. https://doi.org/10.4319/lo.2008.53.5.1784

Lane, T. W., & Morel, F. M. M. (2000). A biological function for cadmium in marine diatoms. In *Proceedings of the national academy of sciences* (Vol. 97, pp. 4627–4631). https://doi.org/10.1073/pnas.090091397

Lemaitre, N., Planquette, H., Dehairs, F., Planchon, F., Sarthou, G., Gallinari, M., et al. (2020). Particulate trace element export in the North Atlantic (GEOTRACES GA01 transect, GEOVIDE cruise). *ACS Earth and Space Chemistry*, *4*(11), 2185–2204. https://doi.org/10.1021/acsearthspacechem.0c00045

Liu, Y., Blain, S., crispi, O., & Obernosterer, I. (2020). Seasonal dynamics of prokaryotes and their associations with diatoms in the Southern Ocean as revealed by an autonomous sampler. *Environmental Microbiology*, *22*(9), 3968–3984. https://doi.org/10.1111/1462-2920.15184

Maarel, M., Marc, J. E. C., Sprenger, W., Haanstra, R., & Forney, L. J. (1999). Detection of methanogenic archaea in seawater particles and the digestive tract of a marine fish species. *FEMS Microbiology Letters*, *173*(1), 189–194. https://doi.org/10.1111/j.1574-6968.1999.tb13501.x

Maldonado, M. T., & Price, N. M. (2001). Reduction and transport of organically bound iron by thalassiosira oceanica (bacillariophyceae). *Journal of Phycology*, *37*(2), 298–310. https://doi.org/10.1046/j.1529-8817.2001.037002298.x

McDonnell, A. M. P., Lam, P. J., Lamborg, C. H., Buesseler, K. O., Sanders, R., Riley, J. S., et al. (2015). The oceanographic toolbox for the collection of sinking and suspended marine particles. *Progress in Oceanography*, *133*, 17–31. https://doi.org/10.1016/j.pocean.2015.01.007

Menden-Deuer, S., & Lessard, E. J. (2000). Carbon to volume relationships for dinoflagellates, diatoms, and other protist plankton. *Limnology & Oceanography*, *45*(3), 569–579. https://doi.org/10.4319/lo.2000.45.3.0569

Moore, R. M., Webb, M., Tokarczyk, R., & Wever, R. (1996). Bromoperoxidase and iodoperoxidase enzymes and production of halogenated methanes in marine diatom cultures. *Journal of Geophysical Research*, *101*(C9), 20899–20908. https://doi.org/10.1029/96JC01248

Morel, F. M. M., Lam, P. J., & Saito, M. A. (2020). Trace metal substitution in marine phytoplankton. *Annual Review of Earth and Planetary Sciences*, *48*(1), 491–517. https://doi.org/10.1146/annurev-earth-053018-060108

Mulrooney, S. B., & Hausinger, R. P. (2003). Nickel uptake and utilization by microorganisms. *FEMS Microbiology Reviews*, *27*(2–3), 239–261. https://doi.org/10.1016/S0168-6445(03)00042-1

Murphy, C. D., Moore, R. M., & White, R. L. (2000). Peroxidases from marine microalgae. *Journal of Applied Phycology*, *12*(3/5), 507–513. https://doi.org/10.1023/A:1008154231462

Ohnemus, D. C., & Lam, P. J. (2014). Cycling of lithogenic marine particles in the US GEOTRACES North Atlantic transect. *Deep Sea Research Part II: Topical Studies in Oceanography*, *116*, 283–302. https://doi.org/10.1016/j.dsr2.2014.11.019

Oliveira, L., & Antia, N. J. (1984). Evidence of nickel ion requirement for autotrophic growth of a marine diatom with urea serving as nitrogen source. *British Phycological Journal*, *19*(2), 125–134. https://doi.org/10.1080/00071618400650131

Planquette, H., & Sherrell, R. M. (2012). Sampling for particulate trace element determination using water sampling bottles: Methodology and comparison to in situ pumps. *Limnology and Oceanography: Methods*, *10*(5), 367–388. https://doi.org/10.4319/lom.2012.10.367

Ploug, H. (2001). Small-scale oxygen fluxes and remineralization in sinking aggregates. *Limnology & Oceanography*, *46*(7), 1624–1631. https://doi.org/10.4319/lo.2001.46.7.1624

Price, N. M., Harrison, G. I., Hering, J. G., Hudson, R. J., Nirel, P. M., Palenik, B., & Morel, F. M. (1989). Preparation and chemistry of the artificial algal culture medium Aquil. *Biological Oceanography*, *6*(5–6), 443–461. https://doi.org/10.1080/01965581.1988.10749544

Prytulak, J., & Elliott, T. (2007). TiO2 enrichment in ocean island basalts. *Earth and Planetary Science Letters*, *263*(3–4), 388–403. https://doi.org/10.1016/j.epsl.2007.09.015

Pullwer, J., & Waniek, J. J. (2020). Particulate trace metal fluxes in the center of an oceanic desert: Northeast Atlantic subtropical gyre. *Journal of Marine Systems*, *212*, 103447. https://doi.org/10.1016/j.jmarsys.2020.103447

Ragueneau, O., Savoye, N., Del Amo, Y., Cotten, J., Tardiveau, B., & Leynaert, A. (2005). A new method for the measurement of biogenic silica in suspended matter of coastal waters: Using Si:Al ratios to correct for the mineral interference. *Continental Shelf Research*, *25*(5–6), 697–710. https://doi.org/10.1016/j.csr.2004.09.017

Rembauville, M., Blain, S., Armand, L., Quéguiner, B., & Salter, I. (2015). Export fluxes in a naturally iron-fertilized area of the Southern Ocean – Part 2: Importance of diatom resting spores and faecal pellets for export. *Biogeosciences*, *12*(11), 3171–3195. https://doi.org/10.5194/bg-12-3171-2015

Rembauville, M., Briggs, N., Ardyna, M., Uitz, J., Catala, P., Penkerc'h, C., et al. (2017). Plankton assemblage estimated with BGC-Argo floats in the Southern Ocean: Implications for seasonal successions and particle export. *Journal of Geophysical Research: Oceans*, *122*(10), 8278–8292. https://doi.org/10.1002/2017JC013067

Rembauville, M., Meilland, J., Ziveri, P., Schiebel, R., Blain, S., & Salter, I. (2016). Planktic foraminifer and coccolith contribution to carbonate export fluxes over the central Kerguelen Plateau. *Deep Sea Research Part I: Oceanographic Research Papers*, *111*, 91–101. https://doi.org/10.1016/j.dsr.2016.02.017

Rembauville, M., Salter, I., Leblond, N., Guéneuguès, A., & Blain, S. (2015). Export fluxes in a naturally iron-fertilized area of the Southern Ocean – Part 1: Seasonal dynamics of particulate organic carbon export from a moored sediment trap. *Biogeosciences*, *12*(11), 3153–3170. https://doi.org/10.5194/bg-12-3153-2015

Ren, H., Brunelle, B. G., Sigman, D. M., & Robinson, R. S. (2013). Diagenetic aluminum uptake into diatom frustules and the preservation of diatom-bound organic nitrogen. *Marine Chemistry*, *155*, 92–101. https://doi.org/10.1016/j.marchem.2013.05.016

da Silva, J. J. R. F., & Williams, R. J. P. (2001). *The biological chemistry of the elements: The inorganic chemistry of life* (2nd ed.). Oxford University Press.

Sternberg, E., Jeandel, C., Miquel, J.-C., Gasser, B., Souhaut, M., Arraes-Mescoff, R., & Francois, R. (2007). Particulate barium fluxes and export production in the northwestern Mediterranean. *Marine Chemistry*, *105*(3–4), 281–295. https://doi.org/10.1016/j.marchem.2007.03.003

Sun, W.-P., Han, Z.-B., Hu, C.-Y., & Pan, J.-M. (2016). Source composition and seasonal variation of particulate trace element fluxes in Prydz Bay, East Antarctica. *Chemosphere*, *147*, 318–327. https://doi.org/10.1016/j.chemosphere.2015.12.105

Sunda, W. G. (2012). Feedback interactions between trace metal nutrients and phytoplankton in the Ocean. *Frontiers in Microbiology*, *3*. https://doi.org/10.3389/fmicb.2012.00204

Taylor, S. R., & McLennan, S. M. (1995). The geochemical evolution of the continental crust. *Review of Geophysics*, *33*(2), 241. https://doi.org/10.1029/95RG00262

Tonnard, M., Planquette, H., Bowie, A. R., van der Merwe, P., Gallinari, M., Desprez de Gesincourt, F., et al. (2020). Dissolved iron in the North Atlantic Ocean and labrador sea along the GEOVIDE section (GEOTRACES section GA01). *Biogeosciences*, *17*(4), 917–943. https://doi.org/10.5194/bg-17-917-2020

Twining, B. S., & Baines, S. B. (2013). The trace metal composition of marine phytoplankton. *Annual Review of Marine Science*, *5*(1), 191–215. https://doi.org/10.1146/annurev-marine-121211-172322

Twining, B. S., Baines, S. B., Fisher, N. S., Maser, J., Vogt, S., Jacobsen, C., et al. (2003). Quantifying trace elements in individual aquatic protist cells with a synchrotron X-ray fluorescence microprobe. *Analytical Chemistry*, *75*(15), 3806–3816. https://doi.org/10.1021/ac034227z

Twining, B. S., Baines, S. B., Vogt, S., & Nelson, D. M. (2012). Role of diatoms in nickel biogeochemistry in the ocean: diatoms and nickel biogeochemistry. *Global Biogeochemical Cycles*, *26*(4), GB004233. https://doi.org/10.1029/2011GB004233

Twining, B. S., Rauschenberg, S., Morton, P. L., & Vogt, S. (2015). Metal contents of phytoplankton and labile particulate material in the North Atlantic Ocean. *Progress in Oceanography*, *137*, 261–283. https://doi.org/10.1016/j.pocean.2015.07.001

Wang, R.-M., Archer, C., Bowie, A. R., & Vance, D. (2019). Zinc and nickel isotopes in seawater from the Indian Sector of the Southern Ocean: The impact of natural iron fertilization versus Southern Ocean hydrography and biogeochemistry. *Chemical Geology*, *511*, 452–464. https://doi.org/10.1016/j.chemgeo.2018.09.010

Weis, D., Frey, F. A., Leyrit, H., & Gautier, I. (1993). Kerguelen archipelago revisited: Geochemical and isotopic study of the southeast province lavas. *Earth and Planetary Science Letters*, *118*(1–4), 101–119. https://doi.org/10.1016/0012-821X(93)90162-3

Yang, H.-J., Frey, F. A., Weis, D., Giret, A., Pyle, D., & Michon, G. (1998). Petrogenesis of the flood basalts forming the northern kerguelen archipelago: Implications for the kerguelen plume. *Journal of Petrology*, *39*(4), 711–748. https://doi.org/10.1093/petroj/39.4.711